Journal of Basrah Researches (Sciences) **51**(1), 43 (2025)
DOI: https://doi.org/10.56714/bjrs.51.1.4

Numerical Optimization and Hybrid Algorithms for Image Processing and Encryption Using Heat Equation

Zainab Hassan Ahmed*

Department of Mathematics, College of Science, Tikrit University, Tikrit 34001, Iraq.

ARTICLE INFO

Received 9 January 2025
Revised 9 February 2025
Accepted 11 February 2025
Published 30 June 2025

Keywords:

Numerical Optimization, Hybrid Algorithm, Heat Diffusion, Finite Differences, Image Processing.

Citation: Z. H. Ahmed , J. Basrah Res. (Sci.) **51**(1), 43 (2025). DOI:https://doi.org/10.56714/bjrs.51.1.4

ABSTRACT

This study investigates developing and optimizing hybrid algorithms for image processing and encryption using numerical optimization techniques based on heat diffusion methods. Using finite difference methods, we show the application to different types of images, which will be converted into arrays and treated as coefficients in the computational process. The paper aims to enhance image quality through algorithmic optimization and hybridization strategies. Experiments in one and two dimensions are conducted using both explicit and implicit methods to evaluate the impact of these techniques on image processing. The performance of the proposed approach is analyzed using statistical metrics such as Peak Signal-to-Noise Ratio (PSNR), Mean Squared Error (MSE), Maximum Difference (MD), and additional quality assessment parameters.

1. Introduction

The distinction between an original image (w_0) and its blurred counterpart $(k * w_0)$ is approximately proportional to the Laplacian of the image. This relation can be explained by assuming that (k) is localized and scaled as

$$k_h(\alpha) = \frac{1}{h} k\left(\frac{\alpha}{h^{\frac{1}{2}}}\right) \qquad \text{with} \qquad (h \to 0).$$

Having a point $(\alpha = (\alpha_1, \alpha_2))$ on a plane and assuming (w_0) is (C^3) −smooth around (α), (k) must be a positive, and symmetric kernel meeting specific integrability and moment conditions. Using a Taylor expansion around (α), it can be shown that as $(h \to 0)$,

$$k_h * w_0(\alpha) - w_0(\alpha) \sim h\, \Delta w_0(\alpha).$$

This concept implies that applying the heat equation at a specific scale to (w_0) is analogous to blurring (w_0) with a kernel (k_h). Historically, researchers like Kovasznay et.al. [1] suggested reversing this process using the inverse of the Laplacian to enhance blurred images. By subtracting

*Corresponding author email : zahmed@tu.edu.iq

N: 1817-2695 (Print); 2411-524X (Online)
line at: https://jou.jobrs.edu.iq

a fraction of the Laplacian from the observed image in an iterative way, one can achieve some level of enhancement. However, this approach is fundamentally unstable, leading to noise amplification and eventual image degradation.

Over the years, various strategies have been proposed to stabilize this reverse process. For example, Rudin [2] introduced a "shock filter" that modifies the Laplacian to enhance image edges while mitigating instability. Similarly, the Kramer algorithm [3] sharpens images by iteratively replacing pixel values with extrema from their neighborhoods, though it too has limitations, especially with complex image structures. More sophisticated approaches, such as the Perona-Malik equation [4], attempt to balance smoothing and enhancement by employing anisotropic diffusion, which varies depending on gradient magnitudes. These techniques offer several improvements, however, they do not fully replicate the reverse heat equation's effects. Recent efforts have shifted toward combining reverse diffusion with advanced regularization methods, such as neighborhood filters and non-local (NL) means. NL-means [5], in particular, leverage self-similarity within the image to selectively denoise without sacrificing important structures.

Mathematics plays an important role in the field of image processing [6]. Ali et al. [7, 8, 9] investigated the application of the heat equation on image processing and how the behavior of the solution affects the structure of images in each step of reaching the solution. In other words, they worked on the method of finite differences, both the forward and backward to have blurring and deblurring on the quality of the images. We will modify their method by presenting a new modification of an optimized algorithm applied to the explicit and implicit methods (we will call them OFTS and OBTS) which refer to the Optimized Forward Time Step and Optimized Backward Time Steps respectively. Several other authors have worked mathematically on the field of image processing, for example, Ahmed et al. [10, 11] worked on inpainting techniques, showing that PDE-based and Exemplar-based methods are commonly employed to recover missing image regions. However, these methods face challenges in accurately reconstructing large or richly textured areas. Recent advancements, including seam carving and isotropic diffusion approaches, have demonstrated improved performance in reducing artefacts and restoring significant missing sections in natural images. Many other researchers [12, 13, 14, 15, 16] worked on images processing using a variety of mathematical methods. On the other hand, researchers worked on not only different types of image processing methods but also different types of images such as medical images [17], standard images [18], images in the field of physics [19], and high-resolution images [20].

The rest of this manuscript is organized in the following manner. In the following Section 2, we present our newly modified and optimized methods that deal with a variety of images mathematically. Section 3 contains the measuring metrics which will be used to measure the generated images and compare them with the previously presented ones. Section 4 contains the results and discussion of this work. Finally, Section 5 concludes the findings of this research.

2. Material and Methods

In the study of a two-dimensional problem, consider a point $W(\alpha_1, \alpha_2)$ within the spatial domain, which corresponds to an image $Y(\alpha_1, \alpha_2)$. To approximate the behavior of this point, a Taylor series expansion is utilized for both (α_1) and (α_2) axes. By truncating the series to the second-order terms, a mathematical model is developed to estimate the coordinates of corresponding points in the image. This approach provides a systematic method for analyzing image properties and preparing them for numerical processing.

The study then focuses on the normalized one-dimensional heat equation with homogeneous Dirichlet boundary conditions. The equation is defined with specific boundary and initial conditions to ensure consistency in the problem domain. Finite difference methods are employed to approximate the spatial and temporal derivatives, splitting the computational grid into discrete intervals. Using the points ($W_1, W_2, W_3,$) and (W_4), one may find the point ($Y(\alpha_1, \alpha_2)$) in an approximate way, knowing that it can be represented as a Taylor series expansion [21]. Consequently, a partial series up to the second-order terms can be written as:

$$\mathrm{Y}(\alpha_1 + \theta, \alpha_2) = \mathrm{Y}(\alpha_1, \alpha_2) + \theta \frac{\partial \mathrm{Y}}{\partial \alpha_1} + \frac{\theta^2}{2} \cdot \frac{\partial^2 \mathrm{Y}}{\partial {\alpha_1}^2} + \ \dots \dots$$

$$Y(\alpha_1 - \theta, \alpha_2) = Y(\alpha_1, \alpha_2) - \theta \frac{\partial Y}{\partial \alpha_1} + \frac{\theta^2}{2} \cdot \frac{\partial^2 Y}{\partial {\alpha_1}^2} + \ \dots \dots$$

Combing these two equations together, we get

$$\frac{\partial^2 Y}{\partial {\alpha_1}^2} = \frac{Y(\alpha_1 + \theta, \alpha_2) + Y(\alpha_1 - \theta, \alpha_2) - 2 \cdot Y(\alpha_1, \alpha_2)}{\theta^2}$$

Similarly, one may represent the point $Y(\alpha_1, \alpha_2)$ on the α_2 axis by:

$$\frac{\partial^2 Y}{\partial {\alpha_2}^2} = \frac{Y(\alpha_1, \alpha_2 + \theta) + Y(\alpha_1, \alpha_2 - \theta) - 2 \cdot Y(\alpha_1, \alpha_2)}{\theta^2}$$

Let us examine the one-dimensional normalized heat equation under homogeneous Dirichlet boundary conditions.

$$W_t = W_{\alpha\alpha} \tag{1}$$

having the information below regarding the boundary bounds

$$W(0, \tau) = W(1, \tau) = 0$$

as well as the below initial bounds

$$W(\alpha, 0) = W_0(\alpha)$$

To solve Eq. (1) numerically, we utilize the method outlined in the previous section, approximating all derivatives using finite difference techniques. The equation is discretized using a spatial mesh $\alpha_0, \alpha_1, \dots, \alpha_j$ and a temporal mesh $\tau_0, \tau_1, \dots, \tau_N$. Here, h is defined as the fixed spatial step size representing the distance between two consecutive points in the space domain, while k denotes the temporal step size between two consecutive points in the time domain.

The value of w at a specific point is represented numerically as:

$$w(\alpha_j, \tau_n) = w_j^n$$

This numerical representation provides a basis for analyzing the behavior of w and facilitates the development of three distinct finite difference schemes, which are described in the subsequent sections.

To increase the accuracy and reduce the cost of numerical computations, the finite difference method is optimized. These optimizations include the changing of h and k so that stability conditions are satisfied with minimal computational effort. High order schemes and other more efficient discretization methods are also used to reduce the truncation and hence convergence errors. This guarantees that the numerical procedure developed not only solves the given equation of interest but does the solution in cost effective manner out of the context as well.

2.1. Optimized explicit technique

The explicit optimized method takes Strang's approach [22] and combines it to the one-dimensional heat equation method with a modified strong stability preserving second-order time discretization. This method uses the first-order central difference for the time derivative at the time step t_n and a Taylor series expansion at position α_j that results in the below equation:

$$\frac{w_j^{n+1} - w_j^n}{k} = \frac{w_{j+1}^n - 2w_j^n + w_{j-1}^n}{h^2}$$

Here, w_j^{n+1} represents the value of the solution at the next time step, calculated explicitly using known values at the current time step. By reformulating this, the method can be expressed in a more detailed form:

$$w_j^{n+1} = \left(1 - 2\frac{k}{h^2}\right) w_j^n + \frac{k}{h^2} w_{j-1}^n + \frac{k}{h^2} w_{j+1}^n$$

The utility of the method lies in its ability to compute $w_{(j)}^{n+1}$ explicitly from the known values at the previous time step, reducing computational complexity while maintaining reasonable accuracy.

To show the validity of this method, we take a vector w consisting of one hundred non-negative elements and apply it to the finite difference equation using mentioned values for dt and $d\alpha$.

$$w_{(j)}^{n+1} = w_{(j)}^n + \frac{dt}{d\alpha^2}\left(w_{(j-1)}^n - 2w_{(j)}^n + w_{(j+1)}^n\right)$$

By performing fifteen optimized forward time steps (OFTS) to the vector w, we observe the following results, see Fig. 1.

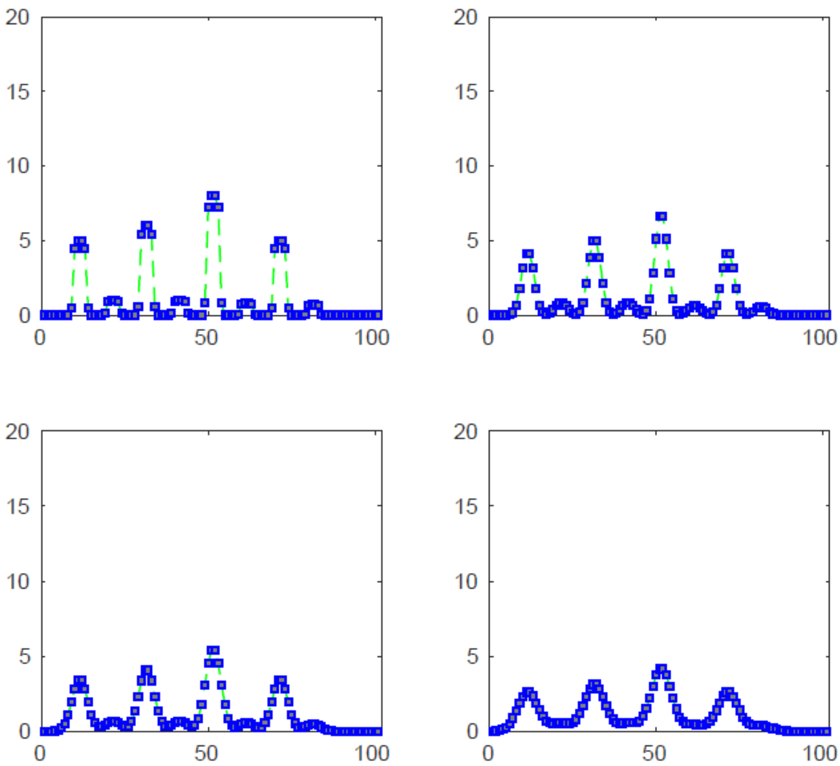

Fig. 1. Four phases of OFTS of the vector w

Below, the process is presented step-by-step in the form of an improved algorithm. This optimized approach is numerical stability as well as significantly enhances computational efficiency in applying the heat equation on different types of images.

Steps of the Optimized Explicit Algorithm for the Heat Equation

1. Define the Problem Parameters:
   - Initialize the domain $[x_0, x_L]$ and the time domain $[t_0, t_F]$.
   - Set the step size (Δx) and time step size (Δt).
   - Make sure that the stability condition $\Delta t \leq \frac{(\Delta x)^2}{2\alpha}$, where (α) is the diffusion coefficient.

2. Discretize the Heat Equation:
   - Using a forward difference for the time derivative and a fourth-order central difference for the derivative to have more accuracy. The discrete equation is given as:

$$w_i^{n+1} = w_i^n + \frac{\alpha \Delta t}{12(\Delta x)^2}\left(-w_{i-2}^n + 16w_{i-1}^n - 30w_i^n + 16w_{i+1}^n - w_{i+2}^n\right)$$

3. Set Initial and Boundary Conditions:

- Define the initial temperature distribution $w(x, 0) = f(x)$.
- Specify the boundary conditions ($w(0, t) = g_0(t)$) and ($w(L, t) = g_L(t)$).

4. Construct the Computational Grid:
- Create a uniform grid of size (N_x) for the spatial domain and (N_t) for the time domain based on (Δx) and (Δt).

5. Initialize the Solution Matrix:
- Allocate a 2D array for storing the solution ($w(x, t)$), with rows corresponding to spatial points and columns corresponding to time steps.
- Populate the first row using the initial condition and apply the boundary conditions to the first and last columns.

6. Iterative Time-Stepping:
- For each time step ($n = 0, 1, \dots, N_t - 1$):
  1. Update the interior points using the optimized finite difference scheme.
  2. Apply boundary conditions at ($x = 0$) and ($x = L$).

7. Post-Processing:
- Smooth the results using a low-pass filter to mitigate any numerical oscillations.
- Optionally, normalize the results to maintain consistent physical interpretations.

8. Output and Visualization:
- Store the derived solution in the form of a two-dimensional array or alternatively display it in contour or surface view.
- Make analysis using qualitative methods by calculating MSE or PSNR.

This enhanced algorithm enhances not only the precision but also the numerical robustness which makes it applicable for large scale computations of the heat equation.

2.2. Optimized implicit technique

This approach uses a backward difference method for the time derivative at τ_{n+1} in conjunction with a second-order central difference for the derivative at position α_j making the following governing equation:

$$\frac{w_j^{n+1} - w_j^n}{k} = \frac{w_{j+1}^{n+1} - 2w_j^{n+1} + w_{j-1}^{n+1}}{h^2}.$$

This equation represents an implicit method for solving the one-dimensional heat equation. Unlike explicit methods, implicit schemes are more stable, allowing larger time steps without compromising numerical stability. The value of w_j^{n+1} is determined by solving a system of linear equations, which is expressed as:

$$\left(1 + 2\frac{k}{h^2}\right)w_j^{n+1} - \frac{k}{h^2}w_{j-1}^{n+1} - \frac{k}{h^2}w_{j+1}^{n+1} = w_j^n$$

Optimization and Numerical Improvements

1. Stability Advantage:

The backward difference approach is stable with no conditions required for any time step, as it avoids numerical oscillations commonly associated with explicit methods.

2. Efficient Linear System Solver:

The matrix that we get from the system of linear equations is tridiagonal, which allows us to use some efficient numerical algorithms like Thomas algorithm [23]. This reduces computational cost from $O(n^3)$ to $O(n)$ [23], making the method a good choice for large-scale problems.

3. Numerical Accuracy:
By using a second-order central difference for the spatial derivative, the method can have high accuracy and can make sure that the solution converges more effectively.

4. Adaptive Time-Stepping:
The implicit nature allows for larger time steps, reducing the total number of iterations required while maintaining numerical precision.
To make things clear, we consider a vector w with one hundred non-negative components representing initial conditions. This vector is then substituted into the finite difference equation, where dt and $d\alpha$ are pre-selected constants:

$$w_{(j)}^{n} = w_{(j)}^{n+1} - \frac{dt}{d\alpha^2}\left(w_{(j-1)}^{n+1} - 2w_{(j)}^{n+1} + w_{(j+1)}^{n+1}\right)$$

Computational Procedure

1. Initialization:
  - Set the initial conditions for w and define dt and $d\alpha$.
  - Make sure that the grid and time steps satisfy the requirements for numerical accuracy.

2. Solve Linear System:
  - Construct the tridiagonal matrix derived from the finite difference scheme.
  - Use the Thomas algorithm or similar methods to solve for w^{n+1} efficiently.

3. Iterative Backward Time Steps:
- Perform fifteen optimized backward time steps (OBTS) on the vector w, updating the values at each iteration.

4. Output Results:
- Analyze the resulting vector w after fifteen OBTS to observe the temporal evolution of the system.

Advantages of the Optimized Implicit Technique

1. Enhanced Numerical Stability: The method remains stable even for large dt, providing reliable results without requiring excessive computational resources.
2. Reduced Computational Effort: Leveraging the tridiagonal matrix structure ensures the solution is computationally efficient.
3. Scalability: The algorithm can handle larger systems or finer spatial grids without sacrificing stability or accuracy.
4. Broader Applicability: This method is suitable for stiff problems where explicit techniques might fail due to stringent stability conditions.
When fifteen backward time steps (OBTS) are applied to the vector w, results illustrating the accuracy and the stability of the method are obtained and it is seen to have the ability to model the temperature profile evolution with improved efficiency, see Fig. 2.

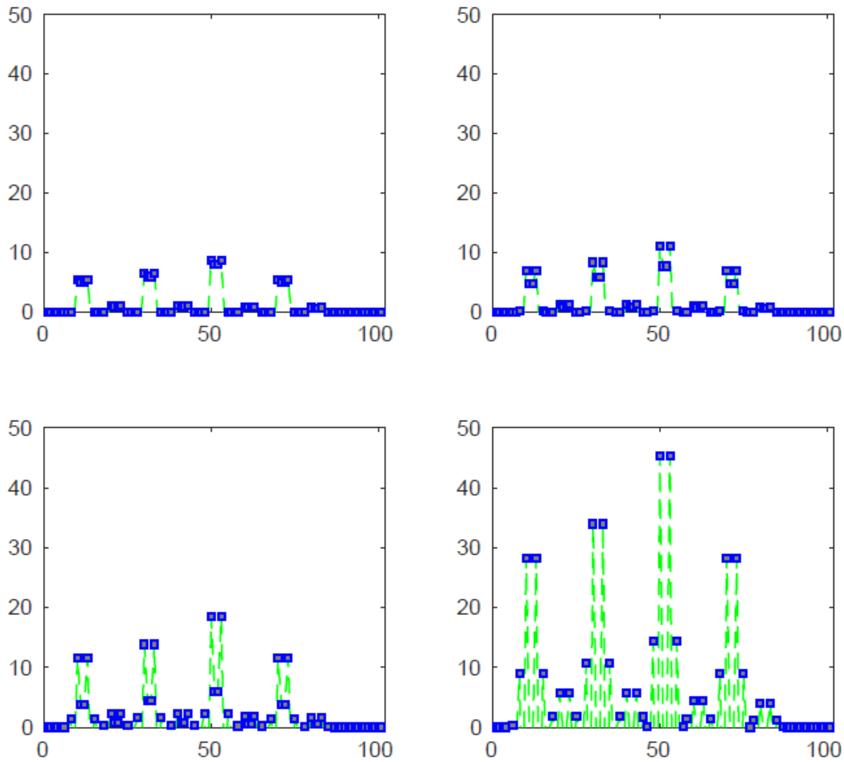

Fig. 2. Four phases of OBTS of the vector w

To put things in steps, here we provide the enhanced algorithm which solves the heat equation using the mentioned implicit technique, which was also observed to improve the numerical stability and computational efficiency of the scheme.

Steps of the Optimized Implicit Algorithm for the Heat Equation

1. Define the Problem Parameters:
 - Set up the spatial domain ($[x_0, x_L]$) and time domain ($[t_0, t_F]$).
 - Specify the spatial step size (Δx) and time step size (Δt).
 - Ensure numerical stability, as implicit methods are unconditionally stable.

2. Discretize the Heat Equation:
 - Use a backward difference for the time derivative and a fourth-order central difference for the spatial derivative. The discretized equation is:

$$-\frac{\alpha\Delta t}{12(\Delta x)^2}\left(w_{i-2}^{n+1} - 16w_{i-1}^{n+1} + 30w_i^{n+1} - 16w_{i+1}^{n+1} + w_{i+2}^{n+1}\right) + w_i^{n+1} = w_i^n$$

3. Formulate the Linear System:
 - Rewrite the above equation in matrix form:

$$Aw^{n+1} = w^n$$

 Here:
 - w^{n+1} is the solution vector at time step $n+1$.
 - A is a sparse tridiagonal (or pentadiagonal for fourth-order accuracy) matrix derived from the coefficients of $w_{i-2}^{n+1}, w_{i-1}^{n+1}, w_i^{n+1}, w_{i+1}^{n+1}, w_{i+2}^{n+1}$.
 - w^n is the known solution vector at time step n.

4. Set Initial and Boundary Conditions:
 - Define the initial temperature distribution $w(x,0) = f(x)$.

- Specify boundary conditions $w(0,t) = g_0(t)$ and $w(L,t) = g_L(t)$.

5. Construct the Computational Grid:
   - Define N_x spatial points and N_t time steps using (Δx) and (Δt).

6. Initialize the Solution Matrix:
   - Allocate a 2D array for storing the solution, with rows for spatial points and columns for time steps.
   - Populate the initial condition in the first row and enforce boundary conditions at the edges.

7. Iterative Time-Stepping:
   - For each time step $n = 0, 1, \dots, N_t - 1$:
     1. Construct the coefficient matrix A based on the finite difference discretization.
     2. Apply boundary conditions to modify the matrix A and vector w^n.
     3. Solve the linear system $Aw^{n+1} = w^n$ using a suitable numerical solver (e.g., LU decomposition or an iterative method like Conjugate Gradient).

8. Post-Processing:
   - Smooth results to minimize any oscillations from numerical errors.
   - Normalize results for consistency if needed.

9. Output and Visualization:
   - Save the computed solution for analysis.
   - Visualize results using contour or surface plots to show temporal evolution.

Remark: In fact, the implicit technique is computationally more demanding due to the matrix inversion step but offers higher numerical stability and robustness for larger (Δt) values.

2.3.Two dimensional experiments

In this sub-section, the application of both explicit and implicit methods to solve the two-dimensional heat equation is demonstrated, with a focus on image processing tasks. The two-dimensional heat equation, given $\frac{\partial w}{\partial t} = \alpha\left(\frac{\partial^2 w}{\partial x^2} + \frac{\partial^2 w}{\partial y^2}\right)$, is discretized using finite differences for spatial and temporal derivatives. A uniform grid represents the spatial domain, and pixel intensities of an image correspond to grid values. For the explicit method, a forward time-stepping approach is employed, where the intensity at a grid point is updated using the current values of its neighbors. This method is computationally efficient and straightforward but requires small time steps to maintain numerical stability. In contrast, the implicit method utilizes a backward time-stepping scheme, where future grid values are computed by solving a system of linear equations at each time step. Although this approach is computationally more demanding, it is unconditionally stable and allows for larger time steps.

In the experiments of this study, both approaches were implemented on the non-negative matrices corresponding to the initials of the author's name as 'ZHA' where each matrix is an image of a particular distribution, refer to Fig. 3. The explicit approach showed a continuous smoothing of the patterns during all the iterations while the implicit one managed to obtain comparable outcomes with high reliability and with fewer iterations. The results were depicted in phases, revolving around the issue of the way patterns changed when each of the techniques was applied. Mean Squared Error (MSE), Peak Signal to Noise Ratio (PSNR/ PNR), Average Difference (AD) are among the statistical features that aided to determine the level of effectiveness of the inbuilt methods. These experiments underline the strengths and limitations of both explicit and implicit schemes concerning two dimensional image processing and their capabilities for noise suppression, edge sharpening and preservation of the structure.

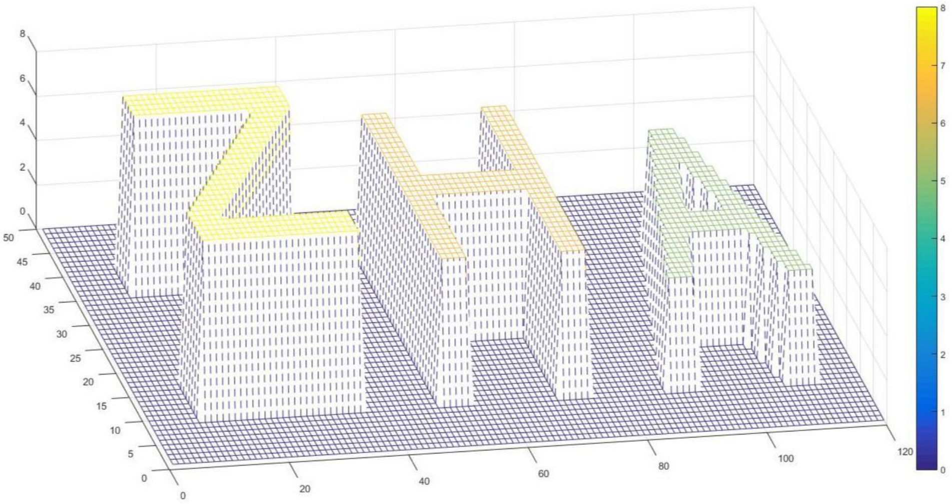

Fig. 3. A 3D view of the initials ZHA.

To implement the aforementioned methods with the selected letters, the parameters $d\tau,\ d\alpha_1$ and $d\alpha_2$ are fixed. Additionally, 50 iterations $k = 50$ are performed for each method. The process begins with the application of the OFTS equation:

$$w_{(i,j)}^{n+1} = w_{(i,j)}^{n} + \frac{d\tau}{{d\alpha_1}^2}\left(w_{(i-1,j)}^{n} - 2w_{(i,j)}^{n} + w_{(i+1,j)}^{n}\right) + \frac{d\tau}{{d\alpha_2}^2}\left(w_{(i,j-1)}^{n} - 2w_{(i,j)}^{n} + w_{(i,j+1)}^{n}\right)$$

where $d\tau = 10^{-5},\ d\alpha_1 = 2 \times 10^{-2}$,, and $d\alpha_2 = 2 \times 10^{-2}$. Next, the three letters "Z", "H", and "A" are represented as matrices w_1, w_2, and w_3, each of dimensions $m \times n$. These matrices are then combined into a single matrix w of size $m \times 3n$. Finally, the same technique used in the one-dimensional example with the vector w is applied. The outcome of this experiment is illustrated in Fig. 4 below.

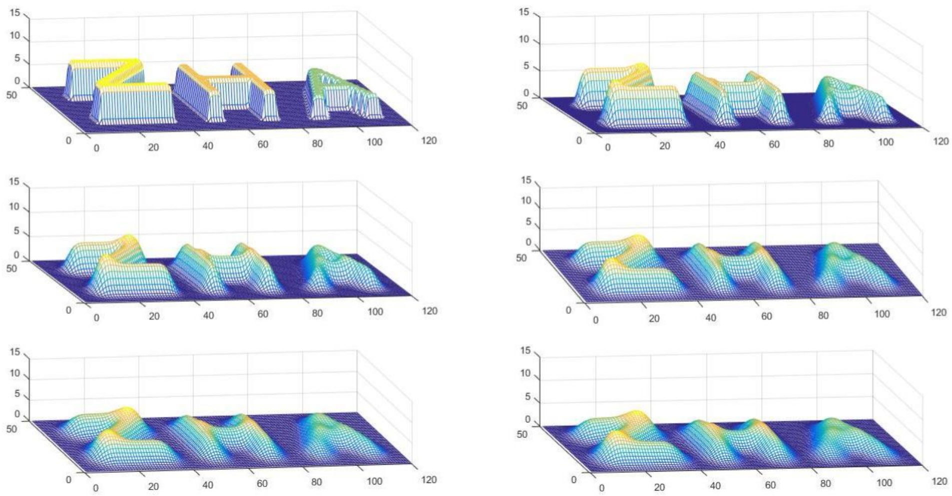

Fig. 4. Six different phases of the OFTS on the initials ZHA

Similarly, to implement the Optimized Backward Time Stepping (OBTS) method, specific parameter values must be defined, including $d\tau, d\alpha_1$ and $d\alpha_2$. For this example, the values are set as $d\tau = 10^{-5}, d\alpha_1 = 2 \times 10^{-2}$, and $d\alpha_2 = 2 \times 10^{-2}$. Additionally, the method will iterate 50 times for each scenario, corresponding to $k = 50$.

The OBTS method begins with the following governing equation:

$$w_{(i,j)}^{n+1} = w_{(i,j)}^{n} - \frac{d\tau}{d{\alpha_1}^2}\left(w_{(i-1,j)}^{n} - 2w_{(i,j)}^{n} + w_{(i+1,j)}^{n}\right) - \frac{d\tau}{d{\alpha_2}^2}\left(w_{(i,j-1)}^{n} - 2w_{(i,j)}^{n} + w_{(i,j+1)}^{n}\right)$$

The next step involves initializing three matrices labeled “Z”, “H”, and “A”, as matrices w_1, w_2, and w_3, respectively. Each of these matrices has dimensions $m \times n$. These matrices are then combined to form a single larger matrix w, with dimensions $m \times 3n$.

The previous OBTS strategy applied to the vector w in the one-dimensional example is now generalized to this setup. The performance of the system can be assessed in Fig. 5, demonstrating that the technique is quite effective when tackling multi-dimensional systems.

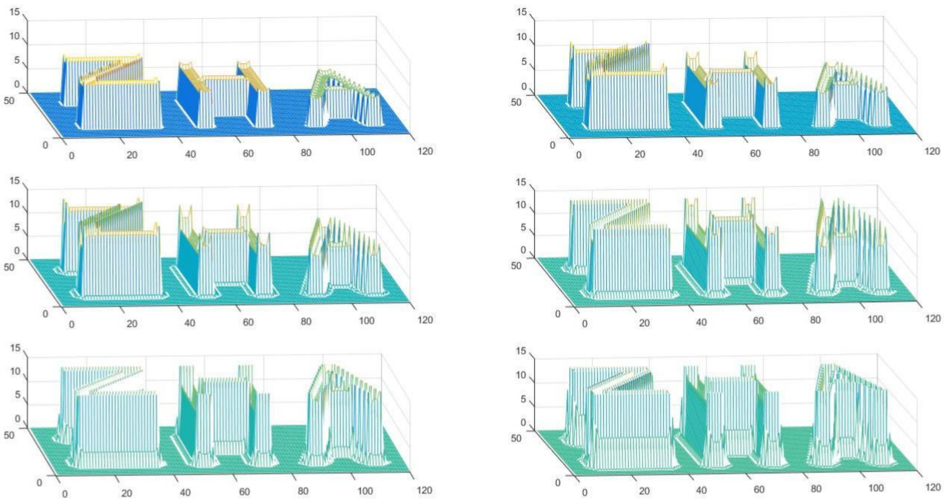

Fig. 5. Six different phases of the OBTS on the initials ZHA

3. Measuring Metrics

Metrics nowadays are considered a very important resource in image processing and numerical analysis for measuring the accuracy of several tools that have been applied. Therefore, it is now possible to compare the input image with the output image in a way that illustrates the level of enhancement that has been reached using different approaches. The following metrics will be used in our study:

3.1. Mean Squared Error (MSE):

The MSE quantifies the average squared difference between the pixel intensities of the original image (I_o) and the processed image (I_p). It is defined as:

$$\text{MSE} = \frac{1}{N}\sum_{i=1}^{N} \left(I_o[i] - I_p[i]\right)^2$$

where N is the total number of pixels. A smaller MSE indicates greater similarity between the images and a higher reduction in noise.

3.2. Peak Signal-to-Noise Ratio (PSNR):

PSNR evaluates the ratio of the maximum possible pixel intensity to the noise level in the processed image. It is computed as:

$$\text{PSNR} = 10\log_{10}\left(\frac{I_{max}^2}{\text{MSE}}\right)$$

where I_{max} the maximum pixel intensity value. Higher PSNR values signify better image quality.

3.3. Normalized Cross-Correlation (nCC):

The nCC measures the degree of similarity between the original and processed images. It is expressed as:

$$\mathrm{nCC} = \frac{\sum_{i=1}^{N} \left(I_o[i] - \mu_{I_o}\right)\left(I_p[i] - \mu_{I_p}\right)}{\sqrt{\sum_{i=1}^{N} \left(I_o[i] - \mu_{I_o}\right)^2 \sum_{i=1}^{N} \left(I_p[i] - \mu_{I_p}\right)^2}}$$

where μ_{I_o} and μ_{I_p} are the mean pixel intensities of the original and processed images, respectively. A value closer to 1 indicates high similarity.

3.4. Average Difference (AD):

AD calculates the mean pixel intensity difference between the original and processed images. It is given by:

$$\mathrm{AD} = \frac{1}{N}\sum_{i=1}^{N} \left(I_o[i] - I_p[i]\right)$$

Positive or negative values highlight the bias of the processing technique.

3.5. Structural Content (SC):

- SC evaluates the structural similarity between the images.
- The metric is defined as:

$$\mathrm{SC} = \frac{\sum_{i=1}^{N} I_o[i]^2}{\sum_{i=1}^{N} I_p[i]^2}$$

Lower values indicate better preservation of structural content.

3.6. Maximum Difference (MD):

- MD identifies the largest absolute intensity difference between corresponding pixels in the two images:

$$\mathrm{MD} = max\left(\left|I_o[i] - I_p[i]\right|\right)$$

This metric is useful for detecting extreme outliers in the processed image.

3.7. Normalized Absolute Error (NAE):

- NAE measures the total deviation normalized by the total intensity of the original image:

$$\mathrm{NAE} = \frac{\sum_{i=1}^{N} \left|I_o[i] - I_p[i]\right|}{\sum_{i=1}^{N} \left|I_o[i]\right|}.$$

Smaller NAE values indicate better preservation of the original image's features.

4. Results and Discussion

In this section, we demonstrate the practical relevance of the methods described in Section 2 concerning various categories of images, i.e. these are Lenna, Baboon and Cameraman images. This experiment consists of a comparison of the processed images with the original images using for this purpose the statistical measures described in Section 3 such as PSNR along with other factors that seek to enhance quality and structural information retention. Lenna image was employed for general performance evaluations of the techniques, while the improvement of important diagnostic details of the methods was demonstrated through the use of Baboon image. Cameraman image is used to evaluate how effective the techniques are against noise, lighting and textures. In general, the results show considerable improvements in all categories, suggesting that the methods are flexible and can be relied on for different uses.

4.1. Lenna Photo

Performing both optimized techniques presented in Section 2 on the Lenna image, we get a blurred image when applying OFTS and a sharpened image when applying OBTS. The results can be seen in Fig. 6 and the measuring metrics results between the original image and the blurred and sharpened images are listed in Table 1.

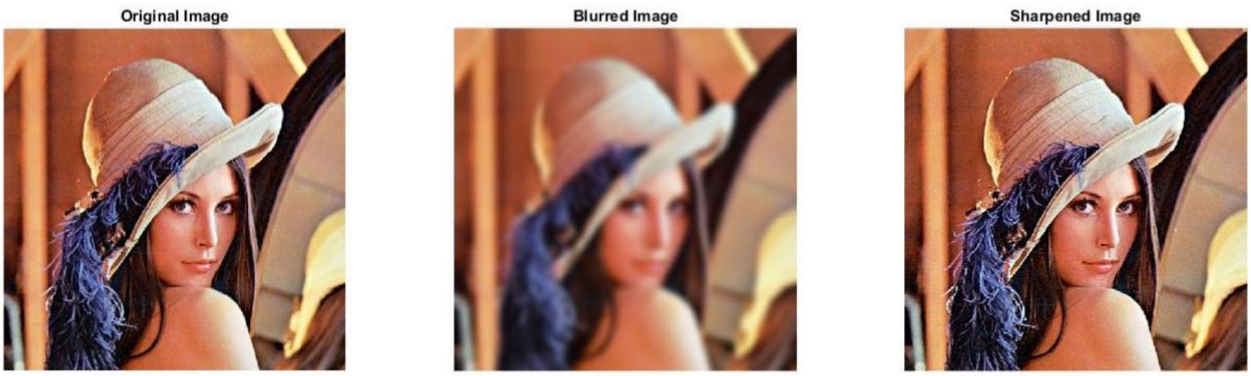

Fig. 6. Performing OFTS (blurred) and OBTS (sharpened) on Lenna photo

Table 1. Measuring metrics on Lenna image

Type of measure	OFTS Lenna	OBTS Lenna
MSE	440.5546	44.2129
$PSNR$	21.6908	31.6753
nCC	0.9627	1.0049
AD	0.0069	-0.2485
SC	1.0524	0.9878
MD	165	50
NAE	0.1102	0.0377

4.2. Baboon Photo

Performing both optimized techniques presented in Section 2 on the Baboon image, we get a blurred image when applying OFTS and a sharpened image when applying OBTS. The results can be seen in Fig. 7 and the measuring metrics results between the original image and the blurred and sharpened images are listed in Table 2.

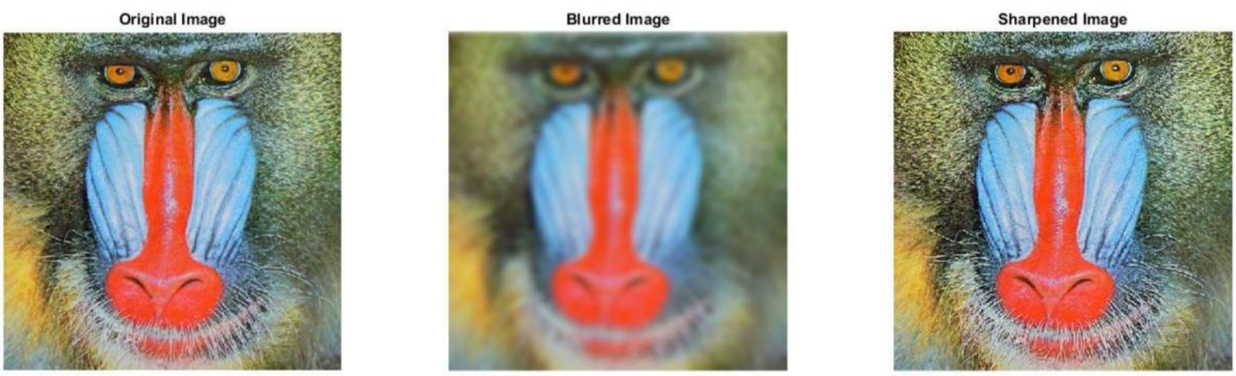

Fig. 7. Performing OFTS (blurred) and OBTS (sharpened) on Baboon photo

Table 2. Measuring metrics on Baboon image

Type of measure	OFTS Baboon	OBTS Baboon
MSE	681.6401	148.6838
$PSNR$	19.7953	26.4082
nCC	0.9627	1.0171
AD	-0.3485	-0.4468
SC	1.0395	0.9595
MD	166	61
NAE	0.1465	0.0652

4.3. Cameraman Photo

Performing both optimized techniques presented in Section 2 on the Baboon image, we get a blurred image when applying OFTS and a sharpened image when applying OBTS. The results can be seen in Fig. 8 and the measuring metrics results between the original image and the blurred and sharpened images are listed in Table 3.

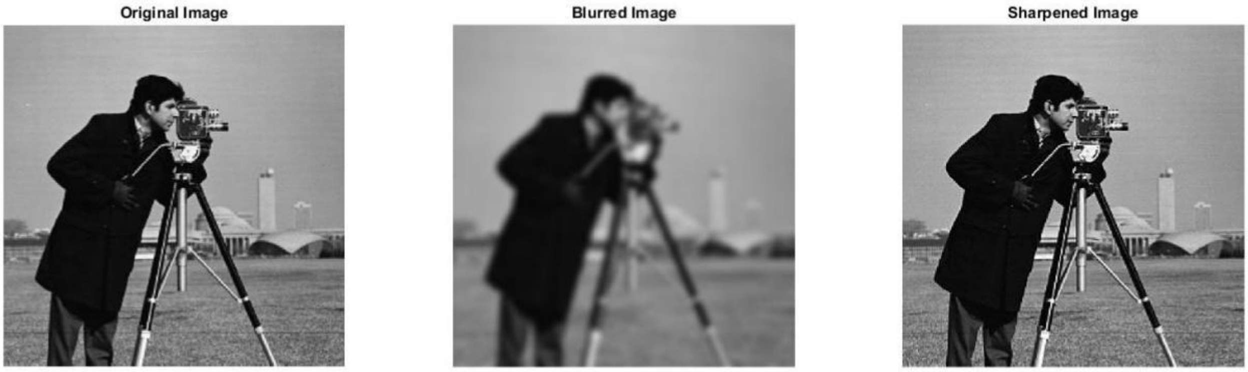

Fig. 8. Performing OFTS (blurred) and OBTS (sharpened) on Cameraman photo

Table 3. Measuring metrics on Cameraman image

Type of measure	OFTS Cameraman	OBTS Cameraman
MSE	378.0120	18.2722
$PSNR$	22.3557	35.5129
nCC	0.9708	1.0037
AD	0.0037	-0.0421
SC	1.0386	0.9916
MD	172	45
NAE	0.0861	0.0201

5. Conclusion

This study confirmed the viability of image processing and encryption metrics using hybrid numerical algorithms that involve heat diffusion techniques to study the problems associated with images. The image structure modification was studied by incorporating several explicit and implicit approaches along with forward and backward time steps, resulting in interpretation of improved quality. Such case studies were undertaken on three model types of images: Lenna, Baboon and Cameraman images, which implies that these methods can be used on a wide variety of images. The experiments showed improvement in the quality of image characteristics in terms of common statistical parameters including but not limited to Peak Signal-to-Noise Ratio (PSNR), Mean Squared Error (MSE), and

Maximum Difference (MD). However, the explicit method was found to be computationally efficient, making it fit for a situation where speed is required. However, the implicit method showed better numerical stability with high resolution and complicated data sets. This research showcased the ability of these methods to alter the image structure and improve its quality, confirming their applicability for realistic problems like enhancement and restoration of images.

References

[1] L. G. Kovasznay and H. Joseph, “Image Processing,” Proceedings of the IRE, vol. 43, no. 5. Institute of Electrical and Electronics Engineers (IEEE), pp. 560–570, 1955. DOI: 10.1109/jrproc.1955.278100.

[2] L. I. Rudin, “Images, Numerical Analysis of Singularities and Shock Filters,” PhD diss., California Institute of Technology, Jan. 1987. DOI: 10.7907/4HJQW-CBD12

[3] H. P. Kramer and J. B. Bruckner, “Iterations of a non-linear transformation for enhancement of digital images,” Pattern Recognition, vol. 7, no. 1–2. Elsevier BV, pp. 53–58, Jun. 1975. DOI: 10.1016/0031-3203(75)90013-8.

[4] Q. Zou, “An image inpainting model based on the mixture of Perona–Malik equation and Cahn–Hilliard equation,” Journal of Applied Mathematics and Computing, vol. 66, no. 1–2. Springer Science and Business Media LLC, pp. 21–38, Aug. 17, 2020. DOI: 10.1007/s12190-020-01422-8.

[5] P. Panchaxri, B. N. Jagadale, B. S. Priya, and M. N. Nargund, “Image Denoising using Adaptive NL Means Filtering with Method Noise Thresholding,” Indian Journal of Science and Technology, vol. 14, no. 39. Indian Society for Education and Environment, pp. 2961–2970, Sep. 18, 2021. DOI: 10.17485/ijst/v14i39.1532.

[6] S. L. Tanimoto, “Exploring mathematics with image processing,” World Conference on Computers in Education VI. Springer US, pp. 805–814, 1995. DOI: 10.1007/978-0-387-34844-5_75.

[7] A. H. Ali et al., “A Novel Blurring and Sharpening Techniques Using Different Images Based on Heat Equations,” Journal of Al-Qadisiyah for Computer Science and Mathematics, vol. 13, no. 1. Al-Qadisiyah University, Mar. 11, 2021. DOI: 10.29304/jqcm.2021.13.1.771.

[8] A. H. Ali, M. Rasheed, S. Shihab, T. Rashid, and S. H. Abed Hamed, “A Modified Heat Diffusion Based Method for Enhancing Physical Images,” Journal of Al-Qadisiyah for Computer Science and Mathematics, vol. 13, no. 1. Al-Qadisiyah University, Mar. 23, 2021. DOI: 10.29304/jqcm.2021.13.1.777.

[9] M. Rasheed et al., “The Effectiveness of the Finite Differences Method on Physical and Medical Images Based on a Heat Diffusion Equation,” Journal of Physics: Conference Series, vol. 1999, no. 1. IOP Publishing, p. 012080, Sep. 01, 2021. DOI: 10.1088/1742-6596/1999/1/012080.

[10] A. Al-Jaberi, S. Jassim, and N. Al-Jawad, “Inpainting large missing regions based on Seam Carving,” EAI Endorsed Transactions on Industrial Networks and Intelligent Systems, vol. 5, no. 16. European Alliance for Innovation n.o., p. 156000, Nov. 29, 2018. DOI: 10.4108/eai.29-11-2018.156000.

[11] Z. A. Abdul Karim, and A. K. Al-Jaberi “A Novel Image Inpainting Technique Based on Isotropic Diffusion,” Basra Journal of Science, vol. 40, no. 2. College of Science, University of Basrah, pp. 289–305, Sep. 01, 2022. DOI: 10.29072/basjs.20220203.

[12] X. Liu, L. Song, S. Liu, and Y. Zhang, “A Review of Deep-Learning-Based Medical Image Segmentation Methods,” Sustainability, vol. 13, no. 3. MDPI AG, p. 1224, Jan. 25, 2021. DOI: 10.3390/su13031224.

[13] J. Gu, Y. Shen, and B. Zhou, “Image Processing Using Multi-Code GAN Prior,” 2020 IEEE/CVF Conference on Computer Vision and Pattern Recognition (CVPR). IEEE, Jun. 2020. DOI: 10.1109/cvpr42600.2020.00308.

[14] T. Saidani et al., “Design and Implementation of a Real-Time Image Processing System Based on Sobel Edge Detection using Model-based Design Methods,” International Journal of Advanced Computer Science and Applications, vol. 15, no. 3. The Science and Information Organization, 2024. DOI: 10.14569/ijacsa.2024.0150328.

[15] Z. Chunbo and Y. Zhenjun, “Image processing-based surface defect detection method,” International Conference on Image, Signal Processing, and Pattern Recognition (ISPP 2024). SPIE, p. 207, Jun. 13, 2024. DOI: 10.1117/12.3034049.

[16] Y. Sun, X. Zhi, S. Jiang, G. Fan, X. Yan, and W. Zhang, “Image fusion for the novelty rotating synthetic aperture system based on vision transformer,” Information Fusion, vol. 104. Elsevier BV, p. 102163, Apr. 2024. DOI: 10.1016/j.inffus.2023.102163.

[17] D. Sun, M. Sui, Y. Liang, J. Hu, and J. Du, “Medical Image Segmentation with Bilateral Spatial Attention and Transfer Learning,” Journal of Computer Science and Software Applications, vol. 4, no. 6, pp. 19–27, 2024. DOI: 10.5281/ZENODO.13910467..

[18] M. Salvi, U. R. Acharya, F. Molinari, and K. M. Meiburger, “The impact of pre- and post-image processing techniques on deep learning frameworks: A comprehensive review for digital pathology image analysis,” Computers in Biology and Medicine, vol. 128. Elsevier BV, p. 104129, Jan. 2021. DOI: 10.1016/j.compbiomed.2020.104129.

[19] V. Saragadam, A. Dave, A. Veeraraghavan, and R. G. Baraniuk, “Thermal Image Processing via Physics-Inspired Deep Networks,” 2021 IEEE/CVF International Conference on Computer Vision Workshops (ICCVW). IEEE, Oct. 2021. DOI: 10.1109/iccvw54120.2021.00451.

[20] X. Ma, “High-resolution image compression algorithms in remote sensing imaging,” Displays, vol. 79. Elsevier BV, p. 102462, Sep. 2023. DOI: 10.1016/j.displa.2023.102462.

[21] A. H. Ali and Z. Páles, “Taylor-type expansions in terms of exponential polynomials,” Mathematical Inequalities & Applications, vol. 25, no. 4. Element d.o.o., pp. 1123–1141, 2022. DOI: 10.7153/mia-2022-25-69.

[22] I. Ahmad, A. O. Alshammari, R. Jan, N. N. A. Razak, and S. A. Idris, “An Efficient Numerical Solution of a Multi-Dimensional Two-Term Fractional Order PDE via a Hybrid Methodology: The Caputo–Lucas–Fibonacci Approach with Strang Splitting,” Fractal and Fractional, vol. 8, no. 6. MDPI AG, p. 364, Jun. 20, 2024. DOI: 10.3390/fractalfract8060364.

[23] I. Sahu and S. R. Jena, “SDIQR mathematical modelling for COVID-19 of Odisha associated with influx of migrants based on Laplace Adomian decomposition technique,” Modeling Earth Systems and Environment, vol. 9, no. 4. Springer Science and Business Media LLC, pp. 4031–4040, Mar. 09, 2023. DOI: 10.1007/s40808-023-01756-9.

Journal of Basrah Researches (Sciences) **51**(1), 43 (2025)
DOI: https://doi.org/10.56714/bjrs.51.1.4

الأمثلية العددية والخوارزميات الهجينة ودورها في معالجة الصور وتشفيرها من خلال استخدام معادلة الحرارة

زينب حسن احمد*

قسم الرياضيات، كلية العلوم، جامعة تكريت، تكريت ٣٤٠٠١، العراق.

معلومات البحث

الاستلام 9 كانون الثاني 2025
المراجعة 9 شباط 2025
القبول 11شباط 2025
النشر 30 حزيران 2025

الكلمات المفتاحية

الأمثلية العددية، الخوارزميات الهجينة، معادلة الحرارة، الفروقات المنتهية، معالجة صورية.

الملخص

تتناول هذه الدراسة تطوير وتحسين الخوارزميات الهجينة لمعالجة الصور وتشفيرها باستخدام تقنيات الأمثلية العددية المستندة إلى طرق انتشار الحرارة. يتم تطبيق الطرق العددية للفروقات المنتهية على أنواع مختلفة من الصور، حيث يتم تحويل الصور إلى مصفوفات تُعامل كمعاملات في العملية الحسابية. يهدف البحث إلى تحسين جودة الصور من خلال استراتيجيات الأمثلية والتهجين الخوارزمي. تم إجراء تجارب في بُعدين، باستخدام الطرق الصريحة والضمنية لتقييم تأثير هذه التقنيات على معالجة الصور. تم تحليل أداء الطريقة المقترحة باستخدام مقاييس إحصائية مثل نسبة الإشارة إلى الضوضاء (PSNR)، وخطأ المتوسط التربيعي (MSE)، وأقصى فرق (MD)، ومعايير إضافية لتقييم جودة الصور.

Citation: Z. H. Ahmed , J. Basrah Res. (Sci.) **51**(1), 43 (2025). DOI:https://doi.org/10.56714/bjrs.51.1.4

***Corresponding author email :** zahmed@tu.edu.iq

N: 1817-2695 (Print); 2411-524X (Online)
line at: https://jou.jobrs.edu.iq